Detection of variance changes and mean value jumps in measurement noise for multipath mitigation in urban navigation

Mariana Spangenberg, Vincent Calmettes, Julien Olivier, Jean-Yves Tourneret, Grégoire Duchâteau

Detection of variance changes and mean value jumps in measurement noise for multipath mitigation in urban navigation

Mariana Spangenberg, Vincent Calmettes, Olivier Julien, Jean-Yves Tourneret, *Senior Member, IEEE*, and Grégoire Duchâteau

Abstract

This paper investigates an urban navigation filter for land vehicles. Typical urban canyon phenomena due to multipath and GPS outages seriously degrade positioning performance. To deal with these scenarios a hybrid navigation system using GPS and dead-reckoning sensors is presented. This navigation system is complemented by a two-step detection procedure that aims at classifying outliers according to their associated source of error. Two different situations will be considered in the presence of multipath. These situations correspond to the presence or absence of line of sight signal for the different GPS satellites. Therefore, two kinds of errors are potentially "corrupting" the pseudoranges, modeled as variance changes or mean value jumps in noise measurements. An original multiple model approach is proposed to detect, identify and correct these errors and provide a final consistent solution.

I. Introduction

Personal land navigation is becoming one of the most widely spread global navigation satellite system (GNSS) applications. In particular, vehicle navigation is nowadays part of many people's daily life. New navigation-based services are demanding higher precision solutions in more challenging environments. Different types of obstacles such as high buildings, trees or tunnels, create an important degradation in the precision of the estimated position. In urban canyon scenarios two main problems have to be considered: a partial or total outage in the satellite visibility, and the lack of reliability in the received pseudorange measurement.

Usual strategies employed by commercial receivers to verify the quality of the received signals are based on integrity checks. If any outlier is present, due for example to a clock failure, the integrity system aims at detecting

Mariana Spangenberg is with the University of Toulouse, TéSA/Thales Alenia Space, 14-16 Port St Etienne, 31000, Toulouse, France, e-mail: mariana.spangenberg@tesa.prd.fr. Vincent Calmenttes is with the Dept. of Electronics and Physics, University of Toulouse, ISAE/TéSA, 10 av. Edouard Belin, BP 54032, 31055 TOULOUSE cedex 4, France, e-mail: vincent.calmettes@isae.fr. Olivier Julien is with the Signal processing and Telecommunications laboratory, University of Toulouse, Ecole Nationale de l'Aviation Civile, 7 Avenue E. Belin, 31055 Toulouse, France, e-mail: ojulien@recherche.enac.fr. Jean-Yves Tourneret is with the University of Toulouse, IRIT/ENSEEIHT/TéSA, 2 rue Camichel, BP 7122, 31071 Toulouse cedex 7, France, e-mail: Jean-Yves.Tourneret@enseeiht.fr. Grégoire Duchâteau is with the Navigation Business Unit, Thales Alenia Space, 26 Avenue Jean-François Champollion, BP 33787, Toulouse, France, e-mail: gregoire.duchateau@thalesaleniaspace.com

This work was supported by Thales Alenia Space, Toulouse, France

its presence. This test is based on a receiver autonomous integrity monitoring (RAIM) strategy for detecting the "defective" signals [1]. However, this approach was conceived for aviation purposes under hypotheses that cannot be always applied to urban vehicle navigation. For instance, a minimum number of unbiased measurements is needed in order to do this integrity check. This condition cannot be ensured in urban canyon scenarios. Moreover, the RAIM is usually complemented by a fault detection and exclusion (FDE) strategy. This strategy enables not only the detection but also the identification and further exclusion of outliers. However, if more than one outlier is present, the capabilities of the FDE to exclude them and provide a reliable solution will be also restricted by the total number of visible satellites. Within this context, this paper proposes a modified "reliability strategy" adapted to urban areas where visibility is reduced and the presence of outliers is mainly due to multipath interference.

Several methods can be found in the literature concerning multipath mitigation. Different configurations of antenna arrays are among the hardware solutions [2], [3]. Working on the receiver correlator output to mitigate the impact of multipath during tracking is another well known approach [4], [5]. However, all these strategies are characterized by their high complexity. In order to avoid these difficulties (and be hardware-independent), multipath mitigation can be performed on the position computation stage (i.e., after the pseudorange calculation). Each "defective" pseudorange is considered to be affected by an error that represents the total contribution of all the multipath signals to the measurement computation.

To address the multipath detection and correction problem Giremus et al. [6] studied a Rao Blackwellized particle filter based on a jump Markov system. This approach consisted of modeling the multipath presence by a mean value jump on the pseudorange whose magnitude was jointly estimated with the vehicle position and velocity. Another two-hypothesis Bayesian approach was considered in [7]. The interfered signals were characterized by error models based on Gaussian mixtures and the tracking was performed using particle filtering. However, the existing algorithms described above require to define a priori distributions for the errors. This a priori knowledge is not easy to obtain in real urban scenarios. Moreover, the high computational cost of particle filters is a problem for land vehicle applications.

This paper proposes to consider two different kinds of errors depending on the conditions in which the GPS signal is received. Reflected signals can arrive to the receiver either in a line-of-sight (LOS) situation where the direct path is present (i.e., direct visibility over the corresponding satellite), or in a non-line-of-sight (NLOS) situation where the received signal contains reflected components only. In particular, this paper will assume that in this latter case just the strongest reflected signal is significant. Thus, the proposed algorithm aims at detecting and classifying pseudorange errors, depending on the reception condition, in order to provide consistent measurements.

A conventional extended Kalman filter (EKF) is considered for determining the navigation solution. This filter is coupled with a two step approach for the detection and correction of errors affecting the received measurements. This approach is based on a hierarchical structure corresponding to a three hypothesis model. A first check is performed to detect the presence of erroneous measurements using the EKF innovations. The second step consists of classifying the different sources of errors depending on the presence or absence of direct signal. Once the type

of error has been identified, the algorithm proceeds to its compensation.

Dead reckoning sensors (DR) are also studied as an augmentation of the proposed system. Accelerometers, gyrocopes and odometers are found among the most popular sensors for land vehicle navigation. They are not affected by space propagation phenomena or radio-frequency (RF) channel impairments such as multipath, and they provide accurate short term precision [8]. The “autonomous integrity monitoring extrapolation” [9] and the “multiple solution separation” [10] are examples of integrity schemes that use inertial information to improve fault detection and exclusion functions. However they were developed according to civil aviation requirements and their functioning and assumptions are not directly suitable for land vehicle navigation. In this paper, the performance of the proposed detection/identification/correction multipath algorithm will be tested in the presence of dead reckoning sensors. Odometric data obtained from the already on board anti-lock braking system (ABS) and gyroscopic data will be used to improve tracking performance.

The paper is organized as follows: Section II briefly introduces multipath phenomenon for urban navigation. Section III describes the navigation filtering models for urban scenarios. The standard RAIM+FDE approach to deal with integrity problems is presented in section IV. Section V discusses the different conditions in which the signal is received and its associated errors. The proposed multiple hypothesis algorithm for multipath interference mitigation is also presented. Sections VI and VII provide a deeper analysis about the detection/identification/correction approach. DR measurements and their contribution to the error control strategy are presented in section VIII. Section IX is devoted to the analysis of experimental results obtained using simulated and real data. Conclusions and suggested future works are finally reported in Section X.

II. Multipath interference

In urban areas, the signal emitted from a satellite is very likely to get reflected and to follow different paths before arriving to the receiver. Therefore, a sum of different and attenuated delayed replicas is usually present in the received signal. For satellite navigation purposes, only the direct signal is useful while the multipath components are considered as undesired signals.

In the presence of multipath the pseudorange measurements will be affected by errors [11], [12]. In order to detect the presence of an anomaly in the pseudorange measurement, the actual error distribution will be studied and contrasted to the nominal error distribution due to the sole presence of noise. Therefore, several pseudorange samples will be needed. Though instantaneously a pseudorange might seem affected by a bias, within an observation window, this error can remain constant or vary over time. This phenomenon will depend on the characteristics of the received reflected signal at each time instant, that themselves depend on the navigation scenario and vehicle dynamics. This paper proposes to consider two kinds of errors affecting the GPS pseudoranges modeled as mean value jumps and variance changes in the additive noise. The first kind of error was studied in [13] for the aerial navigation while the second type of error was considered in [14], [15]. To validate these two hypotheses Fig. 1 presents results for a real test field campaign done an urban area. The displayed results were obtained from a 25

minute and 5.6 km campaign held in Toulouse centre, France (for more details please refer to section IX-B). The pseudorange errors for two different satellites are shown in the top figures. The probability distribution functions (*pdf*s) of the normalized errors (i.e., errors divided by their corresponding noise standard deviations) are displayed in the bottom figures. In open sky scenarios the normalized pseudorange errors follow a Gaussian distribution [16]. Conversely, the bottom figures show that the Gaussian density assumption is not valid for the considered satellites. In Fig. 1(c) the noise variance seems to be underestimated by the fitted Gaussian pdf, whereas Fig. 1(d) shows a mean shifted pdf. Note that the pseudorange errors presented similar characteristics in [7] and [17] under different conditions.

Hereafter, errors introduced in the pseudorange measurement by the presence of reflected signals will be referred to as the NLOS case (when the presence of a reflected signal in the absence of the direct signal introduces a mean value jump) and the LOS case (when both multipath and the direct signal are present and a noise variance jump is induced). In the NLOS case, only a reflected signal is received and tracked (a constant bias is present in the pseudorange measurement). In the LOS case, the measurement is composed by the direct signal plus delayed reflections. Considering that the tracking is done for a moving vehicle, the multipath signal amplitude, phase and time of arrival will rapidly vary over time. Hence, the value and sign of the introduced errors will be constantly changing and this situation will be modeled by a noise variance jump. Indeed, the actual mean value jump does not only represent a NLOS situation but also an LOS situation where the vehicle is not moving (i.e., the multipath amplitude, delay and phase are constant, so its final contribution to the direct received signal is also a mean value jump). However, as this error is finally considered under the hypothesis $\mathcal{H}_1$, the approach is still valid without loss of generality. The following section makes explicit the relation between these two types of errors and the received measurement model.

III. General Navigation models

A. State Model

The state equation considered in this paper for the GPS navigation filter is

$$X_t = \Phi_t X_{t-1} + v_t, \tag{1}$$

where X_t is the state vector, Φ_t the state transition matrix and v_t is the system noise vector. The state vector includes the following parameters:

$$X_t = (\lambda_t, \phi_t, h_t, v_{n,t}, v_{e,t}, v_{d,t}, b_t, d_t)^T, \tag{2}$$

where (λ_t, ϕ_t, h_t) describes the vehicle position in earth-centered earth-fixed (ECEF) geodetic coordinates (i.e., latitude, longitude and height), and $(v_{n,t}, v_{e,t}, v_{d,t})$ contains the vehicle velocities in the north-east-down (NED) frame. The receiver clock bias and drift are denoted as (b_t, d_t) respectively. The noise vector v_t in (1) corresponds to a random walk model where the acceleration has a zero mean Gaussian distribution modeled by the system

noise covariance matrix Q_t. The acceleration variances associated to $(v_{n,t}, v_{e,t}, v_{d,t})$ are denoted as $\left(\sigma_n^2, \sigma_e^2, \sigma_d^2\right)$ where $\sigma_n^2 = \sigma_e^2$ and $\sigma_d^2 << \sigma_n^2$. This variance choice considers no a-priori knowledge on the vehicle privileged direction and no important changes in the vehicle altitude (which is usually the case in dense urban areas). Details on the NED to ECEF frame transformation can be found in [18, page 191].

B. Measurement Model

The pseudorange measurement model associated to the ith satellite can be written as

$$Y_{t,i} = \left\|p_{t,i}^s - p_t\right\| + b_t + \boldsymbol{m}_{t,i} + \sqrt{(\sigma_{t,i}^2 + \boldsymbol{r}_{t,i}^2)} w_{t,i}, \tag{3}$$

where $Y_{t,i}$ is the ith *corrected* pseudorange measurement associated to the ith visible GPS satellite for $i = 1, ..., n_y$ (n_y being the number of visible satellites) and $p_{t,i}^s = (x_{t,i}^s, y_{t,i}^s, z_{t,i}^s)$ is the ith GPS satellite position expressed in ECEF rectangular coordinates. Note that the term *corrected* was used for the pseudorange because ionosphere, troposphere, ephemeris and satellite clock errors are considered to be already compensated in (3) (using EGNOS or WAAS for instance). The vehicle position vector expressed in ECEF rectangular coordinates is denoted as p_t. It is obtained from the state variables (λ_t, ϕ_t, h_t) with an appropriate frame transformation (for more details see [18, ch. 2]). The receiver clock bias is denoted as b_t, while $\sigma_{t,i}^2$ is the measurement noise variance in nominal conditions for the ith satellite, and $w_{t,i}$ is a zero mean Gaussian variable such that $w_{t,i} \sim \mathcal{N}(0, 1)$. The possible multipath errors are denoted as $\boldsymbol{m}_{t,i}$ and $\boldsymbol{r}_{t,i}^2$, where $\boldsymbol{m}_{t,i}$ represents a mean value jump for the ith satellite (i.e. a departure from the nominal mean value in eq. (3) given by $\left\|p_{t,i}^s - p_t\right\| + b_t$) and $\boldsymbol{r}_{t,i}^2$ a respective noise variance jump (i.e. a departure from the nominal measurement variance given by $\sigma_{t,i}^2$). The n_y measurements are usually concatenated according to

$$Y_t = \mathrm{h}(X_t) + M_t + R_t^{1/2} w_t \tag{4}$$

where $Y_t = (Y_{t,1}, ..., Y_{t,n_y})^T$ is the measurement vector, and $\mathrm{h}(X_t) = \|p_t^s - p_t\| + b_t$ represents the measurement function including a frame transformation from the geodetic state coordinates to the rectangular coordinates. The mean value jump vector $M_t = (m_{t,1}, ..., m_{t,n_y})^T$ is such that $m_{t,i} \neq 0$ if the ith satellite is affected by a mean jump and $m_{t,i} = 0$ otherwise. Assuming the pseudoranges are independent, the measurement noise covariance matrix R_t is expressed as

$$R_t = \mathrm{diag}\left[\left(\sigma_{t,1}^2 + \boldsymbol{r}_{t,1}^2, \ldots, \sigma_{t,n_y}^2 + \boldsymbol{r}_{t,n_y}^2\right)\right], \tag{5}$$

where the diag operator denotes a diagonal matrix, and $\boldsymbol{r}_{t,i} \neq 0 \ \ \forall i = 1, \ldots, n_y$ if the ith satellite is affected by a noise variance jump and $\boldsymbol{r}_{t,i} = 0$ otherwise.

IV. INTEGRITY STRATEGY: SNAPSHOT RAIM+FDE

Integrity is generally defined as a measure of the trust that can be placed in the correctness of the information supplied by a system. In accordance, an error bound is a measure of trust on the accuracy of the estimation. Among the different existing integrity procedures, the snapshot RAIM is the best known and widely implemented approach [1]. The FDE is a complement to this system where not only the presence of an anomaly is detected but its source (i.e., the corresponding satellite) is identified and excluded. The weighted least square (WLS) estimator of the state vector at time instant t, derived from the measurement model in (4), is defined as

$$\widehat{X}_t = \widehat{X}_{t-1} + \Delta\widehat{X}_t, \tag{6}$$

with

$$\Delta\widehat{X} = (H_t^T R_t^{-1} H_t)^{-1} H_t^T R_t^{-1} \Delta Y_t,$$

$$\Delta Y_t = Y_t - \mathrm{h}(\widehat{X}_{t-1}),$$

where H_t is the linearized measurement matrix around $\widehat{X}_{t-1}$ and $\widehat{X}_{t-1}$ is the previous value of the state vector. The vector of WLS residuals is defined as:

$$e_t = Y_t - \mathrm{h}(\widehat{X}_t) = \Delta Y_t - \left[\mathrm{h}(\widehat{X}_t) - \mathrm{h}(\widehat{X}_{t-1})\right] = \left[\mathbb{I}_{n_y} - H_t(H_t^T R_t^{-1} H_t)^{-1} H_t^T R_t^{-1}\right] \Delta Y_t.$$

where $\mathbb{I}_{n_y}$ is the $n_y \times n_y$ identity matrix. Different test statistics can be used with the snapshot RAIM strategy to detect an anomaly. The range comparison method [19], the least square (LS) residual method [20] and the parity method [21] are three of the main snapshot RAIM algorithms that use different test statistics. Due to its low computational cost, the LS residual method is going to be used in this paper. The corresponding test statistics is defined as:

$$\mathrm{SSE} = e_t e_t^T = \|e_t\|^2 . \tag{7}$$

where SSE stands for sum of the squared errors. The test statistics SSE follows a χ^2 distribution with $n_y - 4$ degrees of freedom [22]. Therefore a minimum of 5 satellites is needed to perform the integrity test. However its detection capability presents many drawbacks. For instance, as the state vector used to compute the residuals was initially computed using the received "defective" measurements, an assimilation of the error might already be present in $\widehat{X}_t$. Especially in the occurrence of large or multiple biases, a compensation might be done within the residuals so the abnormal situation is finally not detectable. This occurs because when computing the residual term (7), a projection of ΔY_t is done on the null space of H_t^T [22]. If the combination of measurement errors is such that the angle between ΔY_t and this subspace is big enough, many information will be lost in the projection. The norm of the residual vector e will be small and the error detection will fail.

The exclusion procedure is performed after an error detection has been achieved. The classical assumption used by the snapshot RAIM+FDE approach is that just *one* outlier can be present. A total of n_y subsets each containing

$n_y - 1$ satellites is built. For this purpose a minimum of 6 satellites must be available. A fault detection condition is performed over the n_y subsets as in the detection step. Just the subset excluding the outlier will be under a given fault detection threshold. Therefore, this subset will be kept to compute the final position estimation.

V. Multipath mitigation approach

A. Multi-hypothesis approach

Usual multipath mitigation schemes based on pseudorange measurements consider a binary system where the received signals are either bias-free or subjected to a multipath interference [6], [7]. In this paper we propose to further develop the interference processing by introducing two different models for LOS and NLOS cases. The assumption considering an error introduced by the presence of multipath is decomposed in order to identify the specific source of this error. Although a change in the noise variance (i.e., LOS case) does not have such a strong impact on the positioning accuracy when compared to a mean value jump, it reveals to be a crucial factor when a precise bounding must be given for the final position solution. As a consequence, we propose a three hypothesis model to detect, identify and correct measurement errors due to multipath:

- $\mathcal{H}_0$: absence of error (only the direct signal is tracked and nominal $\sigma^2_{t,i}$ is considered to correctly model the pseudorange zero-mean measurement noise),

$$m_{t,i} = 0, \qquad r^2_{t,i} = 0. \tag{8}$$

- $\mathcal{H}_1$: the received measurement is in NLOS situation and affected by a mean value jump,

$$m_{t,i} \neq 0, \qquad r^2_{t,i} = 0. \tag{9}$$

- $\mathcal{H}_2$: the received measurement is in LOS situation and is affected by a variance change in the additive noise,

$$m_{i,t} = 0, \qquad r^2_{i,t} \neq 0. \tag{10}$$

Under hypothesis $\mathcal{H}_0$, the model error (i.e., the additive noise) has a Gaussian distribution. However, under hypotheses $\mathcal{H}_1$ and $\mathcal{H}_2$, the nominal Gaussian distribution is no longer valid because of multipath presence. [1] The errors associated to the two hypotheses $\mathcal{H}_1$ and $\mathcal{H}_2$ were modeled as Gaussian mixtures in [7]. However, when analyzed more in detail, these mixture models (obtained from a real navigation scenario) can also be decomposed into a mean-shifted or a variance-increased Gaussian distribution (see Fig. 4 of [7]). This decomposition considerably facilitates the analysis when compared to a Gaussian mixture model. Indeed, determining the number of components participating in a Gaussian mixture is fairly complicated.

[1] A fourth hypothesis associated to multiple NLOS signals but no LOS signal situation and defined by non zero m and r might also be considered. However, including this hypothesis would significantly increase the algorithm complexity. Since this hypothesis has a very small probability compared to $\mathcal{H}_0$, $\mathcal{H}_1$ and $\mathcal{H}_2$, it has not been considered in this study.

B. System outline

Due to the non linearity of the measurement model in (3) an EKF is used for the general navigation solution. A hierarchical method is proposed for error detection and later for error identification and correction. The idea is that this multi-stage approach enables an urban-adapted navigation filter without entailing heavy computations in clear sky scenarios. This multi-stage scheme can be summarized as follows:

1) **Error detection**:

   The presence of an error is detected by performing a statistical test on the innovations.

2) **Error identification**:

   In case an error has been detected, a parallel processing is achieved for classifying the two possible sources of error. Two "time of occurrence" tests are performed simultaneously for the detected outliers. These outliers can be affected by a mean value jump or by a variance change in the additive noise. The most likely hypothesis ($\mathcal{H}_1$ or $\mathcal{H}_2$) is then considered for error correction.

3) **Error correction**:

   The innovation model is updated by correcting either the noise mean value or the noise variance, depending on the hypothesis that has been detected in the identification step. The corrected model is then fed back to the main system (composed by the EKF) that computes the final position.

A block diagram for the proposed detection/identification/correction system is depicted in Fig. 2.

C. EKF innovations

The proposed multi hypothesis approach can detect outliers, identify and correct different types of errors. The detection of measurement errors will be conducted by using the EKF innovations

$$I_t = Y_t - Y(\widehat{X}_{t|t-1}), \tag{11}$$

where $I_t = (I_{t,1}, ..., I_{t,n_y})^T$ is the EKF innovation vector and $Y(\widehat{X}_{t|t-1}) = \mathrm{h}(\widehat{X}_{t|t-1})$ is the vector containing the pseudorange measurements predicted from the propagated state vector (see [23] and [24] for similar approaches). In nominal condition (hypothesis $\mathcal{H}_0$), the innovations are distributed according to a zero mean Gaussian distribution whose covariance matrix S_t is defined as

$$S_t = H_t P_{t|t-1} H_t^T + R_t, \tag{12}$$

where H_t is the linearized measurement matrix around $\widehat{X}_{t|t-1}$ (according to (4)), $\widehat{X}_{t|t-1}$ is the propagated EKF state vector at time t and R_t is computed according to (5) with $r_{t,i}^2 = 0 \; \forall i = 1, ..., n_y$. The a priori state covariance noise matrix is denoted as $P_{t|t-1}$. No correlation is assumed between different satellite measurements. The variance of the ith innovation at time instant t (denoted as $s_{t,i}^2$) is given by the ith element of the diagonal of S_t. As a consequence, the ith innovation error under hypothesis $\mathcal{H}_0$ (i.e., in nominal situation) is distributed according to a

zero-mean Gaussian distribution with variance $s_{t,i}^2$ and pdf

$$p(I_{t,i}|\mathcal{H}_0) = \frac{1}{\sqrt{2\pi}s_{t,i}} \exp\left(-\frac{1}{2s_{t,i}^2} I_{t,i}^2\right). \tag{13}$$

VI. Error detection

The first step of the algorithm detects the presence of corrupted signals referred to as outliers. The type of error affecting the signal is not specified at this point. This hierarchical approach, where the outliers are first detected and their source of error is later identified, is preferred to a strategy where the three hypothesis are simultaneously studied for every received signal because of its lower computational cost (considering that usually the number of received signals largely exceeds the number of outliers). A binary hypothesis test is performed to determine the absence (hypothesis $\mathcal{H}_0$) or presence (hypotheses $\mathcal{H}_1$ and $\mathcal{H}_2$) of an error in the measurements. The test is achieved for each of the n_y received signals through their respective innovations. A test based on the knowledge of the C/N_0 ratio was presented in [7] to decide whether the received signal is error corrupted or not. However, in the $\mathcal{H}_2$ case where the multipath is in phase with the direct signal, this test may no longer be valid. This paper considers a sliding window of N samples as observation window and assumes that the error (when it exists) is constant during this period of time. It is important to notice that the choice of N is always ruled by a trade-off between the sensitivity and detection time of the test. The normalized energy of the innovations for each of the n_y observation windows containing N samples is computed. The detection of errors is then achieved as follows:

$$T_{t,i} = \sum_{j=t-N+1}^{t} \frac{I_{j,i}^2}{s_{j,i}^2} \underset{\mathcal{H}_1 \text{ or } \mathcal{H}_2}{\overset{\mathcal{H}_0}{\lessgtr}} \alpha \qquad \forall i = 1, \ldots, n_y \tag{14}$$

where α is the detection threshold, $I_{j,i}$ and $s_{j,i}^2$ are obtained as explained in the previous section, and $\frac{I_{j,i}}{s_{j,i}}$ represents the normalized measurement innovation. The test statistics $T_{t,i}$ is distributed according to a central chi2 distribution with N degrees of freedom (denoted as χ_N^2), under hypothesis $\mathcal{H}_0$. The detection threshold α is obtained from the probability of false alarm (PFA) of the test as:

$$\alpha = C_{\chi_N^2}^{-1}\left(1 - \text{PFA}\right), \tag{15}$$

where $C_{\chi_N^2}^{-1}(\cdot)$ represents the inverse cumulative distribution function of the χ_N^2 distribution. An accurate estimation of each innovation error distribution under $\mathcal{H}_0$ (i.e., $\mathcal{N}(0, s_{j,i}^2)$) is supposed to be available. The critical factor to obtain a precise value of $s_{j,i}^2$ is the ability to correctly determine the nominal measurement noise variance $\sigma_{t,i}^2$ associated to each ith measurement. Further details on the way this variance is calculated in practice are given in section IX.

If the test statistics $T_{t,i}$ exceeds the threshold α, the presence of an error is declared for the ith measurement and the error estimation procedure is used to determine the kind of error affecting the received measurement. Fig. 3 shows hypothetic innovation error distributions under the hypotheses $\mathcal{H}_0$, $\mathcal{H}_1$ and $\mathcal{H}_2$. It can be seen that the presence of error in the measurements (hypotheses $\mathcal{H}_1$ and $\mathcal{H}_2$) yields innovations with larger energy than

under hypothesis $\mathcal{H}_0$. It is important to note that the threshold determination does not depend on the innovation distributions associated to $\mathcal{H}_1$ and $\mathcal{H}_2$. Moreover, no knowledge about the mean value jumps and the variance changes in the additive noise has to be known to compute the test statistics.

At this point it is necessary to introduce the vector O_t which contains the position of the different detected outliers with respect to the measurement vector Y_t. It is defined as $O_t \subset [1, ..., n_y]$, where $O_t = (O_{t,1}, \ldots, O_{t,n_o}) \in \mathbb{R}^{n_o}$, and n_o denotes the number of detected outliers.

VII. Error identification and correction

Once an *outlier* has been detected, its source of error has to be identified and corrected. Estimates of m and r are simultaneous computed and the most likely type of error is used to determine the final navigation solution. Due to the recursive nature of the EKF, not only the error magnitude has to be estimated but also its time of occurrence. Note that the error magnitude is generally smoothed within the observation window in (14), so that the effective time of detection of the error does not match its real time of occurrence k. In case of miss detection, the error gets propagated through the state vector, and the estimated error magnitude can differ significantly from the real value. As a consequence, both hypotheses $\mathcal{H}_1$ and $\mathcal{H}_2$ depend not only on the error parameter m or r (that are supposed to be constant inside the observation window) but also on the time of occurrence k (where k can take any value within the observation window containing samples from time instant $t - N + 1$ to time t) that should be estimated carefully. Change detection techniques such as the Neyman Pearson test [25, page 33] need to know the model parameters conditionally to each hypothesis in order to provide an optimal solution. Unfortunately, this is not the case in practical applications where neither the time of occurrence of the change nor its magnitude are known. This paper derives a test for error identification appropriate to such situations.

A. Time of occurrence estimation

The time of occurrence estimation can be achieved by using the marginalized likelihood ratio test (MLRT) proposed by Gustafsson [26]. However, this test requires an a priori knowledge about the probability distributions of the parameters to be estimated (mean value jumps or variance changes in our case). In the generalized likelihood ratio test (GLRT) [27] the jump is considered as an unknown constant (as opposed to a random variable). The GLRT proceeds for each of the qth detected outlier to a double maximization over the variable of interest (m or r) and the time of occurrence k. However, implementing the GLRT in our system presents two main drawbacks. On one hand, a bank of N^{n_o} recursive least square filters must be deployed for each hypothesis (considering that the ensemble of outliers follows either $\mathcal{H}_1$ or $\mathcal{H}_2$), which presents a heavy computational cost for systems where the estimation delay must be extremely short. On the other hand, the GLRT proposed in [27] is based on the idea that the relation between the error affecting the measurement and the EKF innovations can be made explicit and represented as a linear regression. However, even if a linear and recursive model can be easily stated for a mean value jump, this is not the case for noise variance changes. Hence, a time of occurrence test adapted to land

navigation phenomena is proposed hereafter where just one filter is deployed for each hypothesis. For the sake of simplicity, the estimation scheme will be developed under the assumption that the whole ensemble of n_o outliers follows either $\mathcal{H}_1$ or $\mathcal{H}_2$. It will be discussed later in this section the performance of the strategy in a more general situation where each outlier is independently affected by $\mathcal{H}_1$ or $\mathcal{H}_2$.

A first estimation of the possible jump magnitudes ($\widehat{m}(k)$ or $\widehat{r}(k)$, $\forall k = t-N+1,\ldots,t$) and their associated log-likelihood ratios ($l\left[k,\widehat{m}(k)\right]$ or $l\left[k,\widehat{r}(k)\right]$, $\forall k = t-N+1,\ldots,t$) is followed by the detection of the time of occurrence $\widehat{k}$. More precisely, the most likely time of occurrence $\widehat{k}_{t,q}$ for hypothesis $\mathcal{H}_1$ is defined as:

$$\widehat{k}_{t,q}(\mathcal{H}_1) = \arg\min_k \left\{k | l_t\left[k,\widehat{m}_{t,q}(k)\right] > \gamma_1\right\}, \tag{16}$$

where $l_t\left[k,\widehat{m}_{t,q}(k)\right]$ is the log-likelihood ratio for the qth outlier ($q = 1,\ldots,n_o$) under hypothesis $\mathcal{H}_1$ at time instant k, and γ_1 is the test threshold that is fixed according to given prior probabilities for hypotheses $\mathcal{H}_1$ and $\mathcal{H}_0$. Once the likelihood function corresponding to a given k overpasses the threshold, $\mathcal{H}_1$ is considered more likely than $\mathcal{H}_0$ at time instant k and thus k is chosen as the time of occurrence of the error (i.e. $\widehat{k}_{t,q} = k$). Indeed, the *smallest* k fulfilling the aforementioned condition is considered as the actual time of occurrence candidate $\widehat{k}_{t,q}$. The estimate $\widehat{m}_{t,q}(k)$ is kept as the actual mean value jump affecting the measurement (considering it remains constant for the rest of the observation window). The estimation of the mean value jump for the qth detected outlier associated to a time of occurrence k is obtained as the mean value of the $(t-k)$th previous EKF innovation samples

$$\widehat{m}_{t,q}(k) = \frac{1}{t-k+1}\sum_{j=k}^{t} I_{j,O_{t,q}}, \qquad \forall k = t-N+1,...,t. \tag{17}$$

where $I_{j,O_{t,q}}$ denotes the nominal $O_{t,q}$th innovation computed under hypothesis $\mathcal{H}_0$ (i.e., $I_{j,O_{t,q}} = I_{j,O_{t,q}}(\mathcal{H}_0)$). It should be noted that eq. (17) is valid under the assumption that a suitable observation window length has been chosen (i.e., the window is long enough to filter the noise contribution and short enough so that the state estimates have not significantly responded to the error). The log-likelihood ratio $l_t\left[k,\widehat{m}_{t,q}(k)\right]$ for every possible time of occurrence k is calculated using the innovation samples at time instant k as follows

$$l_t[k,\widehat{m}_{t,q}(k)] = \log\left[\frac{p\left(I_{k,O_{t,q}}|\mathcal{H}_1\right)}{p\left(I_{k,O_{t,q}}|\mathcal{H}_0\right)}\right], \tag{18}$$

with

$$p\left(I_{k,O_{t,q}}|\mathcal{H}_1\right) = p[I_{k,O_{t,q}}(\mathcal{H}_1)], \tag{19}$$

where $p(I_{k,O_{t,q}}|\mathcal{H}_1)$ represents the $I_{k,q}$ pdf considering an error $\widehat{m}_{t,q}(k)$ at time instant k to be present. The EKF innovation $I_{k,O_{t,q}}(\mathcal{H}_1)$ calculated under hypothesis $\mathcal{H}_1$ is obtained from

$$I_k(\mathcal{H}_1) = Y_k - Y[\widehat{X}_{k|k-1}(\mathcal{H}_1)] - \widehat{M}_k, \tag{20}$$

where $I_k(\mathcal{H}_1)$ is the innovation vector, $I_{k,O_{t,q}}(\mathcal{H}_1)$ is its $O_{t,q}$th element, $\widehat{X}_{k|k-1}(\mathcal{H}_1)$ is the propagated state vector

under hypothesis $\mathcal{H}_1$ and $\widehat{M}_k$ is the mean value jump vector of dimension $n_y \times 1$. The ith element of vector $\widehat{M}_k$ is defined as

- $\widehat{M}_{k,i} = 0$, (non corrupted measurement) if $i \notin O_t$ where O_t is the vector containing the index of all the detected outliers,
- $\widehat{M}_{k,i} = \widehat{m}_{t,q}(k)$, if $i = O_{t,q}$ and the time of occurrence has not yet been detected for the qth outlier,
- $\widehat{M}_{k,i} = \widehat{m}_{t,q}(\widehat{k}_{t,q}(\mathcal{H}_1))$, if $i = O_{t,q}$ and the time of occurrence has already been detected for the qth outlier (i.e., $k > \widehat{k}_{t,q}(\mathcal{H}_1)$).

According to (20), each $I_{k,O_{t,q}}(\mathcal{H}_1)$ follows a Gaussian distribution $\mathcal{N}(0, s^2_{k,O_{t,q}})$, where $s^2_{k,O_{t,q}}$ is calculated under hypothesis $\mathcal{H}_0$ according to (12). The propagated state vector $\widehat{X}_{k|k-1}(\mathcal{H}_1)$ in (20) is computed as $\widehat{X}_{k|k-1}(\mathcal{H}_1) = \Phi_k\, \widehat{X}_{k-1}(\mathcal{H}_1)$, where $\widehat{X}_{k-1}(\mathcal{H}_1)$ is the corrected state vector under hypothesis $\mathcal{H}_1$ at time $k-1$. If no outlier has been detected at $k-1$ then $\widehat{X}_{k-1}(\mathcal{H}_1) = \widehat{X}_{k-1}(\mathcal{H}_0)$. Consider for instance that the first outlier appears at time instant k. Then $\widehat{X}_{k-1}(\mathcal{H}_1) = \widehat{X}_{k-1}(\mathcal{H}_0)$ and $\widehat{X}_k(\mathcal{H}_1)$ is calculated after the corresponding innovation is corrected for the error presence (i.e. the corresponding element of the $\widehat{M}_k$ vector is set to the estimated bias). For every observation window $\widehat{X}_{t-N}(\mathcal{H}_1)$ is initialized as $\widehat{X}_{t-N}(\mathcal{H}_1) = \widehat{X}_{t-N}(\mathcal{H}_0)$. The corrected state vector at time k which depends on $I_k(\mathcal{H}_1)$ and will be used at time $k+1$ for the computation of $\widehat{X}_{k+1|k}(\mathcal{H}_1)$, is obtained from the EKF update state equation as

$$\widehat{X}_k(\mathcal{H}_1) = \widehat{X}_{k|k-1}(\mathcal{H}_1) + K_k I_k(\mathcal{H}_1), \tag{21}$$

where K_k is the EKF gain matrix under nominal conditions (hypothesis $\mathcal{H}_0$) and $I_k(\mathcal{H}_1)$ is obtained from (20). Eqs. (20) and (21) highlight the relation between a correct innovation model and an unbiased position estimation $\Big(\text{contained in } \widehat{X}_k(\mathcal{H}_1)\Big)$ and viceversa.

Similarly to the "time of occurrence estimation" for hypothesis $\mathcal{H}_1$ presented in Eqs. (16) to (19), the most likely time of occurrence for hypothesis $\mathcal{H}_2$ is

$$\widehat{k}_{t,q}(\mathcal{H}_2) = \arg\min_k \left\{k | l_t\left[k, \widehat{r}^2_{t,q}(k)\right] > \gamma_2\right\}, \tag{22}$$

where γ_2 is the test threshold that is fixed according to given prior probabilities for hypotheses $\mathcal{H}_2$ and $\mathcal{H}_0$. The noise variance jump estimation $\widehat{r}^2_{t,q}(k)$ for each possible time of occurrence k is defined as

$$\widehat{r}^2_{t,q}(k) = \frac{1}{t-k+1} \sum_{j=k}^{t} \left[I^2_{j,O_{t,q}} - s^2_{j,O_{t,q}}\right]. \tag{23}$$

The nominal innovation variance $s^2_{j,O_{t,q}}$ (estimated under hypothesis $\mathcal{H}_0$ and obtained from (12)) is subtracted from the calculated innovation variance in order to obtain the noise variance jump associated to the measurement. The log-likelihood ratio for each possible time of occurrence k considering that outliers are affected by an error of type $\mathcal{H}_2$ is defined as

$$l_t[k, \widehat{r}^2_{t,q}(k)] = \log\left[\frac{p\left(I_{k,O_{t,q}}|\mathcal{H}_2\right)}{p\left(I_{k,O_{t,q}}|\mathcal{H}_0\right)}\right], \tag{24}$$

with

$$p\left(I_{k,O_{t,q}}|\mathcal{H}_2\right) = p[I_{k,O_{t,q}}(\mathcal{H}_2)], \tag{25}$$

where $p(I_{k,O_{t,q}}|\mathcal{H}_2)$ represents the $I_{k,O_{t,q}}$ pdf considering an error $\widehat{r}^2_{t,q}(k)$ at time instant k to be present. The EKF innovation $I_{k,O_{t,q}}(\mathcal{H}_2)$ calculated under hypothesis $\mathcal{H}_2$ follows a Gaussian distribution $\mathcal{N}(0, s^2_{k,O_{t,q}}(\mathcal{H}_2))$ such that

$$R_k(\mathcal{H}_2) = \text{diag}(\widehat{\Theta}_k), \tag{26}$$

$$S_k(\mathcal{H}_2) = H_k P_{k|k-1} H_k^T + R_k(\mathcal{H}_2), \tag{27}$$

where $s^2_{k,O_{t,q}}(\mathcal{H}_2)$ corresponds to the $O_{t,q}$th element from the diagonal of $S_k(\mathcal{H}_2)$ and $\widehat{\Theta}_k$ is the measurement noise variance vector whose ith element is defined as

- $\widehat{\Theta}_{k,i} = \sigma^2_{k,i}$, if $i \notin O_t$ (non corrupted measurement),
- $\widehat{\Theta}_{k,i} = \sigma^2_{k,i} + \widehat{r}^2_{t,q}(k)$, if $i = O_{t,q}$ and the time of occurrence has not yet been detected for the qth outlier,
- $\widehat{\Theta}_{k,i} = \sigma^2_{k,i} + \widehat{r}^2_{t,q}(\widehat{k}_{t,q}(\mathcal{H}_2))$, if $i = O_{t,q}$ and the time of occurrence has already been detected for the qth outlier (i.e., $k > \widehat{k}_{t,q}(\mathcal{H}_2)$).

The corrected state vector under hypothesis $\mathcal{H}_2$ is then calculated as

$$\widehat{X}_k(\mathcal{H}_2) = \widehat{X}_{k|k-1}(\mathcal{H}_2) + K_k(\mathcal{H}_2) I_k(\mathcal{H}_2), \tag{28}$$

where the EKF gain matrix $K_k(\mathcal{H}_2)$ under hypothesis $\mathcal{H}_2$ is computed using (27) according to

$$K_k(\mathcal{H}_2) = \frac{P_k H_k^T}{S_k(\mathcal{H}_2)}, \tag{29}$$

and the innovation vector $I_k(\mathcal{H}_2)$ (where $I_{k,O_{t,q}}(\mathcal{H}_2)$ is its $O_{t,q}$th element) is described as follows

$$I_k(\mathcal{H}_2) = Y_k - Y[\widehat{X}_{k|k-1}(\mathcal{H}_2)]. \tag{30}$$

In this way, Eqs. (26) to (30) highlight the dependence among the estimated noise variance parameter $\widehat{r}^2_{t,q}$, the final position solution contained in $\widehat{X}_k(\mathcal{H}_2)$ and the innovations $I_{k,O_{t,q}}(\mathcal{H}_2)$ to be used for the "time of occurrence test" in (24).

Some pertinent remarks are made on the "time of occurrence test" algorithm related to both hypotheses $\mathcal{H}_1$ and $\mathcal{H}_2$ to facilitate the comprehension of the proposed approach:

1) For the computation of $\widehat{X}_k(\cdot)$ all the available n_y innovations are used.
2) Only the innovations associated to the detected n_o outliers are corrected.
3) The innovation vector $I_k(\cdot)$ contains $(n_y - n_o)$ non corrected innovations.

The proposed strategy was presented under the assumption that the whole ensemble of detected outliers was affected by the same type of error. For a more general case, where no correlation among the errors of the measurements is assumed, a straightforward strategy would be to build a bank of 2^{n_o} filters, each of them considering a possible

combination of error sources (mean value or noise variance jump) for the n_o detected outliers. In urban areas where many simultaneous outliers can be present, this solution presents a too high computational cost. However, we will now explain why the above developed strategy is also well suited to independent error measurements. Consider the general case where two measurements are simultaneously corrupted at time instant $(t-d)$ (where $d < N$) and that the error detection (14) is achieved at time instant t. Assume for instance that the first measurement Y_1 is affected by a mean value jump and the second measurement Y_2 is affected by a noise variance jump. At the output of each of the two filters considering exclusively $\mathcal{H}_1$ or $\mathcal{H}_2$ we will obtain:

- **For the $\mathcal{H}_1$ filter**: the $\mathcal{H}_1$time of occurrence test (16) will detect the presence of an error in Y_1 at the $(t-d)$ instant. For Y_1 a mean value jump will correctly compensate the innovation model. However, no mean value jump will be detected for Y_2. According to (17), any possible mean value jump affecting Y_2 will approximately equal zero (because Y_2 was just affected by a noise variance jump). Thus, for any time of occurrence candidate the test in (16) will not overpass the threshold γ_1. As previously stated in the paper, a non corrected noise variance jump affects mainly the covariance matrix of the state vector, not its mean value. Therefore the Y_1 corrected innovations (20) won't be significantly affected by the non detected noise variance jump in Y_2.
- **For the $\mathcal{H}_2$ filter**: the $\mathcal{H}_2$ time of occurrence test (22) will detect an error in the two measurements at $(t-d)$. The innovation model corresponding to Y_2 will be correctly compensated by a jump in the noise variance. The Y_1 innovation model will be compensated by a *fictitious* noise variance jump. The value of this variance jump will be proportional to the actual mean value jump affecting Y_1 (23). In theory, any non detected mean jump entails important biases in the state vector parameters (which will later condition the innovation calculation). However, the contribution of Y_1 to the state vector estimation is inversely proportional to its associated noise variance (i.e., if the noise variance is high, the EKF gain (29) for the measurement innovation will be low). Therefore, potentially high mean value jumps will be deweighted during the $\mathcal{H}_2$ filtering. In this way, the corrected Y_2 innovation model (30) won't be significantly affected by the non-compensated bias in Y_1.

It is important to note that this discussion is valid even if the times of occurrence of the errors are not the same.

B. Error identification

After the time of occurrence detection has been performed in parallel for $\mathcal{H}_1$ and $\mathcal{H}_2$, a decision has to be taken on the actual source of error affecting each outlier (i.e., either $\mathcal{H}_1$ or $\mathcal{H}_2$). Two different situations have to be considered at the output of the time of occurrence test:

1) An error estimation for the qth outlier has been obtained under both hypotheses $\mathcal{H}_1$ (with $\widehat{k}_{t,q}(\mathcal{H}_1), \widehat{m}_{t,q}$) and $\mathcal{H}_2$ (with $\widehat{k}_{t,q}(\mathcal{H}_2), \widehat{r}^2_{t,q}$)
2) The presence of an error for the qth outlier has been detected for only one hypothesis (i.e. for only one of the log-likelihood ratio tests (16) or (22) the threshold has been exceeded).

In the second situation, no further test is required to decide on the measurement error source: the sole hypothesis under which the error has been detected is considered as the actual source of error (mean value jump for $\mathcal{H}_1$ or

noise variance jump for $\mathcal{H}_2$). However, if an error has been detected under both hypotheses, a final solution must be taken regarding the real origin of this error (remember that the measurement is exclusively affected by $\mathcal{H}_1$ or $\mathcal{H}_2$). Assuming both $\mathcal{H}_1$ and $\mathcal{H}_2$ have the same probabilities, the test for deciding between $\mathcal{H}_1$ and $\mathcal{H}_2$ is defined by

$$p\left[I_{t-N+1:t,O_{t,q}}|\widehat{k}_{t,q}(\mathcal{H}_1)\right] \underset{\mathcal{H}_2}{\overset{\mathcal{H}_1}{\gtrless}} p\left[I_{t-N+1:t,O_{t,q}}|\widehat{k}_{t,q}(\mathcal{H}_2)\right] \tag{31}$$

with

$$p\left[I_{t-N+1:t,O_{t,q}}|\widehat{k}_{t,q}(\mathcal{H}_1)\right] = \prod_{j=t-N+1}^{t} p\left[I_{j,O_{t,q}}(\mathcal{H}_1)\right], \tag{32}$$

$$p\left[I_{t-N+1:t,O_{t,q}}|\widehat{k}_{t,q}(\mathcal{H}_2)\right] = \prod_{j=t-N+1}^{t} p\left[I_{j,O_{t,q}}(\mathcal{H}_2)\right], \tag{33}$$

where $I_{t-N+1:t,O_{t,q}} = (I_{t-N+1,O_{t,q}}, ..., I_{t,O_{t,q}})$.

C. Error correction

Once a decision has been taken regarding the source of error affecting each outlier, their associated innovation model has to be corrected and fedback to the update stage of the EKF algorithm. More precisely, if the qth outlier is affected by NLOS errors ($\mathcal{H}_1$) the associated innovation is corrected according to

$$\tilde{I}_{t,O_{t,q}} = I_{t,O_{t,q}} - \widehat{m}_{t,q}\left[\widehat{k}_{t,q}(\mathcal{H}_1)\right], \tag{34}$$

whereas if it is affected by LOS errors ($\mathcal{H}_2$) the measurement variance is corrected as

$$\tilde{\sigma}^2_{t,O_{t,q}} = \sigma^2_{t,O_{t,q}} + \widehat{r}^2_{t,q}\left[\widehat{k}_{t,q}(\mathcal{H}_2)\right], \tag{35}$$

where $\tilde{\sigma}^2_{t,O_{t,q}}$ and $\tilde{I}_{t,O_{t,q}}$ denote the corrected parameters to be updated in the EKF algorithm. In the last case, the corrected measurement variance is used for the new computation of the measurement noise covariance matrix R_t. In this way, a final unbiased navigation solution is calculated. It is important to observe that for the future error detection test in $t+1$ (14), the $\tilde{I}_{t,O_{t,q}}$ term will not replace the original innovation parameter $I_{t,O_{t,q}}$ calculated for $\mathcal{H}_0$. The observation window always contains the non corrected innovations to enable the detection of an error during its whole duration.

VIII. Land navigation system with dead reckoning sensors

A. Principles

During partial and total GPS outages the contribution of dead reckoning (DR) sensors is crucial. They enable continuity over the position estimation. If left alone for a long period, the DR sensors provide highly biased solutions [28]. However, for short GPS outage periods, they can be used as a reliable source of navigation. If the

initial position is known, by integrating the measurements, they can provide a position estimation similarly to an autonomous navigation system. Moreover, as they give a priori information about the vehicle dynamics, GNSS reliability checks as the one proposed in the previous sections can become more efficient. A second navigation system allows the presence of an outlier to be more easily detected. Corrupted pseudorange measurements are not compared to a statistical model of the vehicles dynamics as described by matrix Q_t in section III, but to the solution computed from the real DR measurements. This paper will considers a tightly-coupled GPS/DR integration strategy in an open-loop configuration. We assume that the measurements from two wheel speed sensors (WSS) located in the vehicle rear wheels and a one-dimension gyroscope are available. The WSS provide a measurement of the wheel angular velocities w in rad/s. Assume first that the wheel radii R_{rr} and R_{rl} (where the subindexes refer to the wheel position as either rear right rr or rear left rl) are constant and known. The norm of the vehicle mean speed (in the along track direction) at time t is computed in [29] as

$$|v|_t = \frac{w_{rr}(t)R_{rr} + w_{rl}(t)R_{rl}}{2}. \tag{36}$$

On the other hand a gyroscope is used to provide the angular yaw rate $\dot{\psi}$. By combination of these two types of sensors a self contained land navigation system is obtained. The errors associated to these DR sensors are estimated in a state vector X_t defined as

$$X_t = \left(\delta\lambda_t, \delta\phi_t, \delta h_t, \delta \mathrm{SF}_t, \delta\psi_t, \delta\dot{\psi}_t, b_t, d_t\right), \tag{37}$$

where δ represents the error associated to each parameter, SF_t is the average of the two wheel's scale factors associated to $|v|_t$ and ψ_t is the vehicle effective yaw angle. The transformation frame expression to obtain the variation in the geodetic coordinates (i.e., $\Delta\lambda_t$ and $\Delta\phi_t$) from the along track velocity $|v|_t$ is given by

$$\Delta\lambda_t\left(|v|_t, \psi_t\right) = |v|_t \cos(\psi_t)\frac{1}{R_\lambda + h_t}, \tag{38}$$

$$\Delta\phi_t\left(|v|_t, \psi_t\right) = -|v|_t \sin(\psi_t)\frac{1}{(R_\phi + h_t)\cos(\lambda_t)}. \tag{39}$$

where R_λ is the earth radius of curvature in a meridian at a given latitude λ_t and R_ϕ is the transverse radius (we consider the WGS84 model for which the earth is an ellipsoid). This paper assumes that the vehicle height h_t is known. Once the state vector gets propagated and corrected, the final geodetic position is given by $\lambda_t = \lambda_t^{DR} + \delta\lambda_t$, $\phi_t = \phi_t^{DR} + \delta\phi_t$ and h_t, where the index DR means that the parameters have been calculated by the stand alone DR system (i.e., using the raw DR measurements only).

B. DR innovations

Though the reliability test principle (as already detailed in sections VI and VII) does not change for the augmented system, a slight modification is introduced in the computation of the observation window innovations $I_{j,i}$ used in (14), (17) and (23). The idea is to exploit the immunity of the DR navigation system against multipath effects to

compute these innovations. The N innovation samples corresponding to the observation window are not taken from the already calculated innovations in (11), where the state vector was used to predict the received measurements. Instead, they are recalculated using only the initial state vector at $(t-N)$ and DR measurements for $[t-N+1:t]$ as follows

$$I_{j,i}^{DR} = Y_{j,i} - \tilde{Y}_{j,i}, \tag{40}$$

where

$$\tilde{Y}_{j,i} = \left\| p_{j,i}^{s} - \tilde{p}_j \right\| + b_{t-N} + \sum_{u=t-N+1}^{j} d_{t-N}\Delta t, \tag{41}$$

$$\tilde{p}_j = \left(a_{t-N} + \sum_{u=t-N+1}^{j} \dot{a}_u^{DR}\Delta t \right)_{\text{llh2rec}}, \tag{42}$$

for $j = t-N+1, ..., t$ and $i = 1, ..., n_y$. The expression $(\cdot)_{\text{llh2rec}}$ denotes a frame transformation from geodetic coordinates to rectangular coordinates. In (42), $a_{t-N} = (\lambda_{t-N}, \phi_{t-N})^T$ is the DR vehicle position in the geodetic frame compensated by errors $(\delta\lambda_{t-N}, \delta\phi_{t-N})$ (estimated in X_{t-N}), b_{t-N} and d_{t-N} are respectively the clock bias and drift at time $t-N$, and $\dot{a}_u^{DR}$ is expressed as

$$\dot{a}_u^{DR} = \begin{bmatrix} \Delta\dot{\lambda}_u \left(\tilde{|v|}_u, \tilde{\psi}_u \right) \\ \Delta\dot{\phi}_u \left(\tilde{|v|}_u, \tilde{\psi}_u \right) \end{bmatrix}, \tag{43}$$

with

$$\tilde{|v|}_u = (\text{SF} + \delta\text{SF}_{t-N}) \, |v|_u \,, \tag{44}$$

$$\tilde{\psi}_u = \psi_{t-N} + \delta\psi_{t-N} + \sum_{e=t-N+1}^{u} \left(\dot{\psi}_e + \delta\dot{\psi}_{t-N} \right) \Delta t. \tag{45}$$

Note that $\dot{a}_u^{DR}$ contains the vehicle relative motion $(\Delta\dot{\lambda}_u, \Delta\dot{\phi}_u)$ at time u according to (38) and (39) (calculated from the *corrected* DR measurements in Eqs. (44) and (45)). Indeed, DR measurements are corrected by errors $(\delta\text{SF}_{t-N}, \delta\psi_{t-N}, \delta\dot{\psi}_{t-N})$ estimated at time $t-N$. In this way, potentially biased state parameters resulting from a non detected multipath error within the observation window do not affect (44) or (45). The new covariance matrix S_j^{DR} associated to innovations in (40) does no longer correspond to (12). As the state vector is not corrected by the pseudorange measurements after time $(t-N)$, S_j^{DR} is now iteratively obtained as,

$$S_j^{DR} = H_j \beta_j H_j^T + R_j \tag{46}$$

with

$$\beta_u = \Phi_u \beta_{u-1} \Phi_u^T + Q_u, \qquad \forall u = t-N+1, ..., j \tag{47}$$

where β is initialized as $\beta_{t-N} = P_{t-N}$, P_{t-N} being the updated state covariance matrix of the EKF at time instant $t-N$. The estimated pseudorange measurements $\tilde{Y}_{j,i}$ are obtained according to (41) by propagating an initial position estimation a_{t-N} with $\dot{a}_u^{DR}$. Therefore, a faster and more accurate error detection is achieved. However, it

must be observed that this DR position propagation strategy is independent of the EKF implementation, i.e., the new $I_{j,i}^{DR}$ does not replace the standard EKF innovations (11) at time j and is only used for (14), (17) and (23).

The approach studied in this section presents the advantage of including a second navigation system, not affected by multipath, that enables a more efficient detection/identification/correction strategy. In the following section, the performance of the augmented DR system is tested with real navigation signals and compared to the stand alone GPS approach.

IX. Simulation results

A. Simulated Data

This section validates the proposed detection/estimation algorithm for a stand-alone GPS approach (without DR measurements) using simulated data. A land vehicle trajectory has been generated according to the state model (1) with acceleration standard deviations (*stds*) $\sigma_n = \sigma_e = 2m/s^2$ and $\sigma_d = 0.2m/s^2$ (i.e. these acceleration *stds* apply to both the trajectory generator and the EKF's Q matrix). The received pseudorange measurements correspond to a simulated GPS constellation with nominal noise *std* $\sigma = 12m$ mainly accounting for thermal noise and other possible error sources in urban environments. The number of visible satellites n_y is constant such that $n_y = 7$. There are no changes in the constellation during the simulation period. The satellite constellation is generated from online available GPS almanac data, with a 5° visibility mask. The pseudoranges are supposed to be compensated by any type of atmospheric error. The errors introduced in the measurements have been generated according to the model (3) as follows

- a mean value jump of $40m$ is introduced in the satellite number 1 between $t = 30s$ and $t = 60s$,
- a noise *std* jump of $40m$ affects the same satellite for a time interval of 40 seconds between $t = 100s$ and $t = 140s$,
- a second satellite (satellite number 2) experiences a mean value jump of $40m$ between $t = 110s$ and $t = 150s$.

The simulated errors were introduced to validate and highlight the performance of the proposed navigation filter in terms of error detection and identification efficiency. The first isolated mean value jump on satellite 1 (corresponding to hypothesis H_1) is the type of error that more visibly affects the positioning accuracy. The correct functioning of the filter is tested for this critical situation. A simultaneous appearance of different errors is then studied. Two satellites are corrupted by different types of errors during overlapped time intervals. In this way, the algorithm is tested for its capacity to identify several defective measurements and their corresponding source of error. The threshold for the error detection in (14) has been adjusted in order to obtain PFA $= 10^{-5}$. Based on several tests done using real data, a suitable observation window length of $N = 5$ was used. This choice was motivated by the need to detect fast changing errors and to achieve fast detection times, with no important losses in sensitivity. The data sampling period equals $1Hz$. The estimation of the time of occurrence in (16) or (22) has been achieved with a threshold $\gamma_1 = \gamma_2 = 1$ (considering no a priori knowledge on the error time of occurrence, so both $\mathcal{H}_0$ and $\mathcal{H}_1$ or $\mathcal{H}_2$ are given the same probability within the observation window).

The error detection/identification results for the interfered satellites are presented in Fig. 4. The top figure shows results for satellite 1 and the bottom figure for satellite 2. The strategy reveals a very good performance since the correct error hypothesis ($\mathcal{H}_0$, $\mathcal{H}_1$ or $\mathcal{H}_2$) is almost always detected. Figs. 5 and 6 show the innovation pdfs corresponding to the two corrupted satellites. The nominal Gaussian pdf is depicted as a solid line while the actual normalized pdf for the EKF innovations is shown with bars. The pdfs are obtained from all the available samples of the simulated satellites. Top figures (a) present results for a standard EKF while bottom figures (b) correspond to the enhanced detection/identification/correction algorithm proposed in this paper. The innovations do not have a Gaussian distribution in the first case because the corrupted measurements are not compensated by the filter. Conversely, when errors are corrected with the proposed algorithm, the histograms of the corrected innovations are close to the adjusted Gaussian pdf.

The results for the final estimated position are presented in Fig. 7. The horizontal position errors (in 2D and illustrated with a solid line) are compared to their corresponding bounds (dashed line). The bounds are calculated from the updated EKF state covariance matrix P_t. In particular the eigenvalues $(\lambda_{1,t}, \lambda_{2,t})$, corresponding to the sub-matrix P_t^H formed by just the horizontal covariance error components, are used for the calculation. An overbounding confidence circle is used rather than an ellipse to illustrate the *worst case* [30]. Only one dimension is used for the bound computation, since the cross-track tolerance is usually larger than the along-track tolerance in deep urban canyon scenarios (due to the strong directional characteristics of the visible satellite geometry). In other words, one of the eigenvalues ($\lambda_{1,t}$ or $\lambda_{2,t}$) usually dominates the other one. The biggest eigenvalue corresponding to the worst case dimension is used. Considering a certain PFA_b, the horizontal bound B_t, illustrated in Figs. 7, 9 and 10, is calculated according to

$$B_t = \sqrt{\max\left(\lambda_{1,t}, \lambda_{2,t}\right)}\ C_{\mathcal{N}}^{-1}\left(1 - \frac{\text{PFA}_b}{2}\right), \tag{48}$$

where $C_{\mathcal{N}}^{-1}(\cdot)$ is the inverse cumulative distribution function of the $\mathcal{N}(0,1)$ distribution. Herein, bounds were calculated using a $\text{PFA}_b = 6.10^{-5}$ which corresponds to a confidence level of 4 *stds*. Result for a standard EKF (i.e., without any error control) are depicted in Fig. 7(a), whereas Fig. 7(b) shows results obtained with the proposed detection/identification/correction filter. In the first case (Fig. 7(a)), the final solution is either biased or not bounded during the intervals where errors are present. However, in the second case (Fig. 7(b)) the corrected position estimates are in good agreement with the bound thanks to the enhanced scheme. In particular, the sawtooth effect observed in Fig. 7(b) is due to a few incorrect error identifications during $t = 100s$ and $t = 400s$ for satellite 1, as observed in Fig. 4(b).

B. Experimental data

The previous subsection proved the relevance of the proposed algorithm under totally known conditions. The estimated magnitude and time of occurrence of interferences could be compared to the corresponding known true values. This subsection studies the reliability strategy on real experimental data. Its performances in terms of

position error and correct bounding will be analyzed. Moreover, dead reckoning data resulting from the WSSs and a gyroscope will be used to show the performance gain obtained when the system is augmented with a second navigation reference. The experimental data was obtained from a test field campaign carried out in Toulouse centre (France). The performed circuit shown in Fig. 8 has a duration of 25 minutes. The total distance traveled is 5.6km. EGNOS corrections [30] were used to compensate ionospheric, tropospheric and ephemeris errors. In this way, it can be assumed that only urban phenomena were perturbating the received signal. The Ublox TIM-LP GPS receiver [31] was used at a data rate of 4Hz. A *synchronized position attitude navigation* (SPAN) system composed by a Novatel receiver, with differential GPS (DGPS) approach, and a high accuracy IMAR inertial unit was taken as reference for the navigation solution [32]. Height measurements were also obtained from this system. The instantaneous noise variance $\sigma^2_{t,i}$, that is a crucial factor in the reliability process, is computed as follows

$$\sigma^2_{t,i} = \sigma^2_{i,\text{URA}} + \sigma^2_{i,\text{uire}} + \sigma^2_{i,\text{tropo}} + \sigma^2_{i,\text{rec}}, \tag{49}$$

where the error components are denoted as URA for the user range accuracy (satellite clock and ephemeris error), uire for the user ionospheric range error, tropo for the tropospheric error and rec for the receiver noise. The first three terms in (49) are obtained from the EGNOS corrections whereas the last one is calculated as a function of the signal to noise ratio (C/N_0) [33]. The bound is computed as in (48) with the same $\text{PFA}_b = 6.10^{-5}$. The acceleration *stds* used for the computation of the system noise covariance matrix Q_t are $\sigma_n = \sigma_e = 2m/s^2$ and $\sigma_d = 0.2m/s^2$. The proposed algorithm is compared to the WLS estimator resulting from the snapshot RAIM+FDE approach. The bound for this latter approach is defined as in (48), where the state covariance matrix is calculated as $P_t = (H_t^T R_t^{-1} H_t)^{-1}$. Results obtained with the standard EKF, the snapshot RAIM+FDE strategy (as described in section IV) and the proposed error control algorithm, using only GPS signals for the navigation, are depicted in Figs. 9(a), 9(b) and 9(d). For the used RAIM+FDE system the black points depicted in Figs. 9(b) and 9(c) represent two situations where the integrity monitor is not available. The first case is when there are less than 6 visible satellites which prevents the use of the FDE function. The second corresponds to the presence of more than one outlier in the different satellite channels. In this case, though a problem was detected, none of the $n_y - 1$ satellite subsets can be considered bias-free which prevents the use of the exclusion function. On the other hand, the error values and time instants where anomalies were detected and successfully corrected are shown as a shaded area under the horizontal error curve (for both integrity/reliability approaches). According to these figures the following observations can be done:

- The standard EKF implemented without the proposed detection/identification/correction strategy presents significant errors and inconsistent solutions (that are not within the computed bounds).
- The widely applied snapshot RAIM+FDE solution presents a poor performance in terms of positioning error. The integrity monitor is unavailable during 10% of the time inducing very important errors. For instance, three main errors may be outlined around the time instants t = 600s, t = 950s and t = 1200s. In the first case, the RAIM+FDE does not performed satisfactorily because only 4 satellites are visible. For the other two errors,

the exclusion function could not be performed because multiple outliers were present among the received GPS signals. Moreover, a bound that largely exceeds the real errors entails an excessively big confidence interval.

- The proposed enhanced EKF reliability strategy clearly outperforms the other two algorithms by eliminating aberrant errors (with a final mean error of $7.7m$) and by providing an appropriated bounded solution during 98.8% of the time.

For the augmented GPS+DR system the velocity measurements were obtained from the on board WSS via the control area network (CAN) bus. The velocity data was produced and processed at 50Hz. The WSS noise *std* is $0.1m/s$ and the WSS scale factor error *std* is 3%. An external gyro specially developed for land vehicle navigation (Melexis MLX90609) was used. This gyro works at 70Hz and has an associated noise *std* equal to 23 deg/h and a dynamic bias *std* equal to 19 deg/h. No significant loss of information was found when interpolating the Melexis-gyro data at 50Hz, so as to align the frequency from both DR sensors. The propagation rate of the EKF was set to 50Hz following the sensor frequency. The stand alone EKF (Fig.10(a)) is compared to the enhanced EKF+error control strategy (Fig. 10(b)). A zoom was done for the first 450 seconds to facilitate the comparison between the two techniques. The following observations can be done:

- The hybrid navigation system (GPS+DR) without any error control presents very interesting performances. From the comparison between Figs. 9(a) and 10(a) it can be observed that the highly informative state model, that corresponds to the multipath-free navigation system, minimizes the influence of outliers on the position solution. Indeed, in Fig. 10(a) outliers are strongly filtered due to the high gain given to the DR sensors on the short term. Only in the presence of long lasting errors the solution could eventually drift. However, this is an unusual phenomenon in urban scenarios. Nevertheless, some inconsistent results are found around the time instants t = 40s, t = 200s, t = 700s and t = 1300s.
- The detection/identification/correction strategy (Fig. 10(b)) compensates most of the inconsistent errors in Fig. 10(a) and provides bounded solutions. Moreover, when the error correction function is active (see shaded area under solid line in Fig. 10(a)), the position error is reduced. Though outliers are highly filtered by the system, when corrected, they allow a more accurate solution.
- The contribution of DR sensors to the final enhanced system using the proposed detection/identification/correction algorithm is easily highlighted from the comparison between Figs. 9(d) and 10(b) : the mean positioning error is decreased, peak errors are smoothed and a more precise bounding is achieved. Indeed, the mean error is reduced to $6.8m$ and the solution is bounded during 97.3% of the time. This slight difference between the bounding performance of the GPS and GPS+DR approach might be due to an actual underestimation of the noise values associated to the sensors.

X. Conclusions

This paper presented an enhanced navigation system adapted to urban canyon scenarios. The originality of the proposed approach relies on the way the received signals are processed: a two step procedure is used to detect

multiple outliers and to classify these outliers according to the *different* types of errors affecting the navigation signal. A hierarchical three-hypothesis test was implemented. Two different situations were considered in the presence of multipath. These situations correspond to the presence or absence of line of sight (referred to as LOS and NLOS situations) over the multiple GPS satellites. Therefore two kinds of errors were potentially "corrupting" the pseudoranges, modeled as noise variance or mean value jumps. The time of occurrence and magnitude of these errors were estimated. In this way, realistic measurement models could be obtained. A multiple model EKF was considered as the best adapted solution for this fast-decision/on-line application. An augmented system including speed sensors and a gyroscope was also proposed for the land vehicle solution. The reliability strategy was adapted to exploit the "multipath independence" of these dead reckoning sensors. Simulated and real data validated the relevance of the proposed algorithm. The detection/identification/correction approach did not only overcome the RAIM availability problem but it also enabled a low error, accurate bounded solution.

The authors acknowledge that more extensive test field campaigns will be certainly necessary to provide a full validation of the proposed strategy. At the same time different GPS receivers and DR sensors should be tested. It will be also interesting to speculate about a fourth signal reception hypothesis (in addition to those proposed in section V-A) where both a mean value and noise variance jump are considered. The application of the Student t and Fisher F tests on the innovation vector (to detect mean value jumps and variance changes respectively) is another interesting idea to explore in future works. Future investigations also include the application of the proposed scheme to different areas where similar problems may be encountered. For example, similar errors were considered to affect the mobile communication signals [15]. The proposed strategy could be interesting in this context.

REFERENCES

[1] R. Conley *et al.*, "Performance of stand-alone GPS," in *Understanding GPS principles and applications*, E. Kaplan and C. Hegarty, Eds. Norwood, MA: Artech House, 2006, ch. 7.

[2] C. C. Counselman, "Multipath-rejecting GPS antennas," *Proc. of the IEEE,*, vol. 87, no. 1, pp. 86–91, Jan. 1999.

[3] J. H. Williams, R. J. Davis, and E. N. Rosario, "Multipath mitigation performance of planar GPS adaptive antenna arrays for precision landing ground stations," in *Proc. of ION GPS 2001*, Salt Lake City, UT, Sept. 2001, pp. 1309–1316.

[4] A. V. Dierendonck, P. Fenton, and T. Ford, "Theory and performance of narrow correlator spacing in a GPS receiver," *Navigation*, vol. 39, no. 3, pp. 265–283, 1992.

[5] C. Macabiau, O. Julien, and E. Chatre, "Use of multicorrelator techniques for interference detection," in *Proc. of ION-NTM 01*, Long Beach, CA, Jan. 2001, pp. 353–363.

[6] A. Giremus and J.-Y. Tourneret, "Joint detection/estimation of multipath effects for the global positioning system," in *Proc. ICASSP-05*, Philadelphia, USA, May 2005.

[7] N. Viandier, D. Nahimana, J. Marais, and E. Duflos, "GNSS performance enhancement in urban environment based on pseudo-range error model," in *Position, Location and Navigation Symposium, 2008 IEEE/ION*, Monterey, CA, May 2008.

[8] B. Barshan and H.F.Durrant-Whyte, "Inertial navigation systems for mobile robots," *IEEE Trans. on Robotics and Automation*, vol. 11, no. 3, pp. 328–342, 1995.

[9] J. Diesel and J. Huddle, "GPS/IRS AIME: Certification for sole means and solution to RF interference," in *Proc. of ION GPS-96*, Kansas City, MO, Sept. 1996, pp. 519 – 528.

[10] M. Brenner, "Integrated GPS/inertial detection availability," in *Proc. of ION GPS-95*, Palm Springs, CA, Sept. 1995.

[11] M. Braasch, "Multipath effects," in *Global Positioning System: theory and applications*, B. Parkinson and J. J.J. Spilker, Eds. Washington, D.C.: American Institute of Aeronautics and Astronautics, 1996, vol. 1, ch. 14.

[12] P. Ward, J. Betz, and C. Hegarty., "Interference, multipath, and scintillation," in *Understanding GPS principles and applications*, E. Kaplan and C. Hegarty, Eds. Norwood, MA: Artech House, 2006, ch. 6.

[13] T. Murphy, M. Harris, P. Geren, T. Pankaskie, B. Clark, and J. Burns, "More results from the investigation of airborne multipath errors," in *Proc. of ION GNSS 2005*, Long Beach, CA, Sept. 2005.

[14] A. Giremus, J.-Y. Tourneret, and V. Calmettes, "A particle filtering approach for joint detection/estimation of multipath effects on GPS measurements," *IEEE Trans. Signal Processing*, vol. 55, no. 4, pp. 1275 – 1285, April 2007.

[15] J. Huerta and J. Vidal, "LOS-NLOS situation tracking for positioning systems," in *Proc. SPAWC-06*, Cannes, France, July 2006.

[16] A. Leick, *GPS Satellite Surveying*, 3rd ed. New Jersey: John Wiley and Sons, 2004.

[17] J. Diesel and J. Huddle, "Performance evaluation of fault detection algorithms as applied to automotive localisation," in *Proc. of ENC-08*, Toulouse, France, April 2008.

[18] J. A. Farrell and M. Barth, *The Global Positioning System and Inertial Navigation*. New York: McGraw–Hill, 1999.

[19] Y. Lee, "Analysis of range and position comparison methods as a means to provide gps integrity in the user receiver," in *42nd Institute of Navigation Annual Meeting*, Seattle, WA, June 1986, pp. 1 – 4.

[20] B. Parkinson and P. Axelrad, "Autonomous GPS integrity monitoring using the pseudorange residual," *Navigation*, vol. 35, no. 2, pp. 255 – 274, 1988.

[21] M. Sturza, "Navigation system integrity monitoring using redundant measurements," *Navigation*, vol. 35, no. 4, pp. 483 – 501, 1988.

[22] I. Martini and G. Hein, "An integrity monitoring technique for multiple failures detection," in *Position, Location and Navigation Symposium, 2006 IEEE/ION*, San Diego, CA, April 2006, pp. 450–467.

[23] C. Hajiyev, "Innovation approach based measurement error self-correction in dynamic systems," *Elsevier Measurement Journal*, vol. 39, no. 7, pp. 585–593, 2006.

[24] S. Ryan and G. Lachapelle, "Augmentation of DGNSS with dynamic constraints for marine navigation," in *Proc. of ION GPS-99*, Nashville, TN, Sept. 1999, pp. 1303 – 1314.

[25] H. L. Van Trees, *Detection, Estimation, and Modulation Theory: Part I*. New York: Wiley, 2001.

[26] F. Gustafsson, *Adaptive filtering and change detection*. Wiley and Sons, 2000, ch. 9.

[27] A. S. Willsky and H. Jones, "A generalized likelihood ratio approach to the detection and estimation of jumps in linear systems," *IEEE Trans. Automatic Control*, vol. 21, no. 1, pp. 108–112, 1976.

[28] M. Spangenberg, V. Calmettes, D. Kubrak, and O. Julien, "Optimized low-cost HSGPS/IMU/WSS land vehicle navigation system for urban navigation," in *Proc. of ION GNSS 2007*, Fort Worth, Texas, Sept. 2007, pp. 70 – 79.

[29] N. Svenzén, "Real time implementation of map aided positioning using a Bayesian approach," Master's thesis, Linköpings University, Dec. 2002.

[30] GNSS Tools Team, "PEGASUS: Technical notes on SBAS," Eurocontrol, Tech. Rep., 2003.

[31] *TIM-LP GPS Receiver Module Data Sheet*, U-blox AG, Switzerland, GPS.G3-MS3-02010-H.

[32] *SPAN Technology for OEMV User Manual*, Novatel Inc., Canada, 2007, OM-20000104.

[33] A. V. Dierendonck, "GPS receivers," in *Global Positioning System: theory and applications*, B. Parkinson and J. Spilker, Eds. Washington, D.C.: American Institute of Aeronautics and Astronautics, 1996, vol. 1, ch. 8.

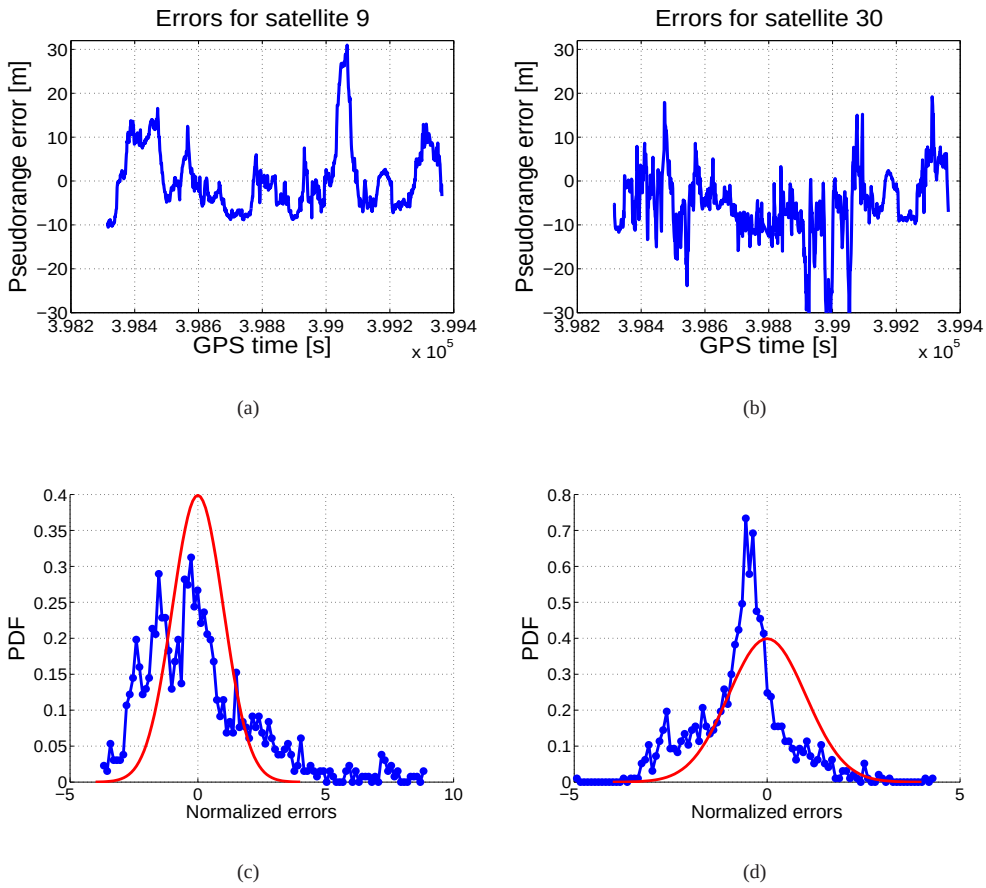

Fig. 1. Pseudorange errors in urban scenarios. (a-b) actual pseudorange errors for two different satellites. (c-d) normalized pseudorange error pdfs (solid-dotted line) and nominal Gaussian pdfs (solid line).

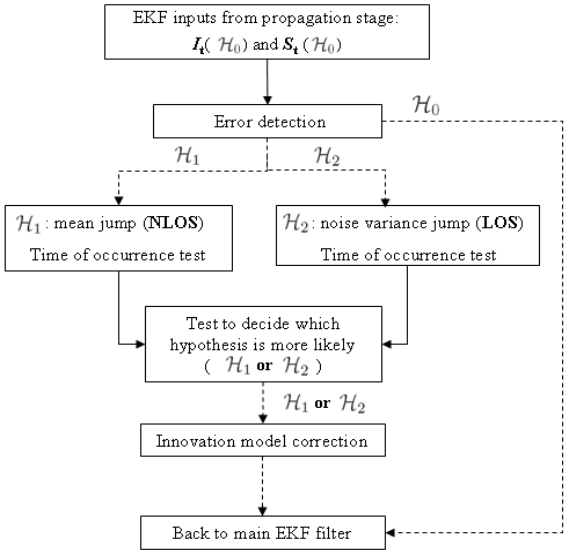

Fig. 2. Proposed strategy for the detection, identification and correction of outliers.

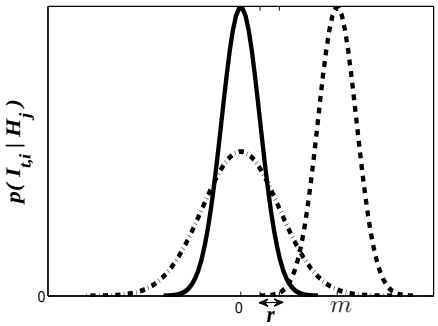

Fig. 3. Innovation pdf $p(I_{t,i}|H_j)$ (solid line for $j = 0$, dashed line for $j = 1$ and dashed-dotted line for $j = 2$).

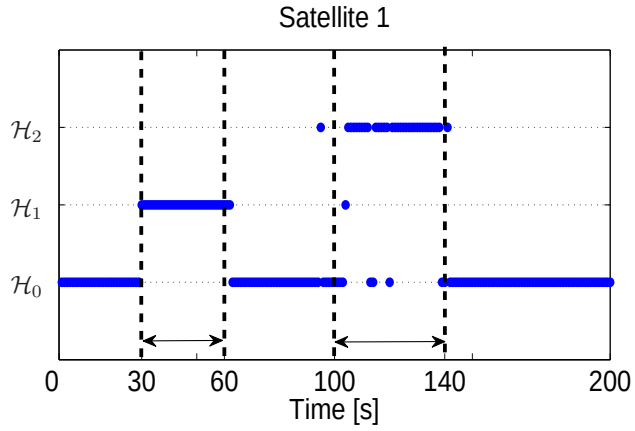

(a)

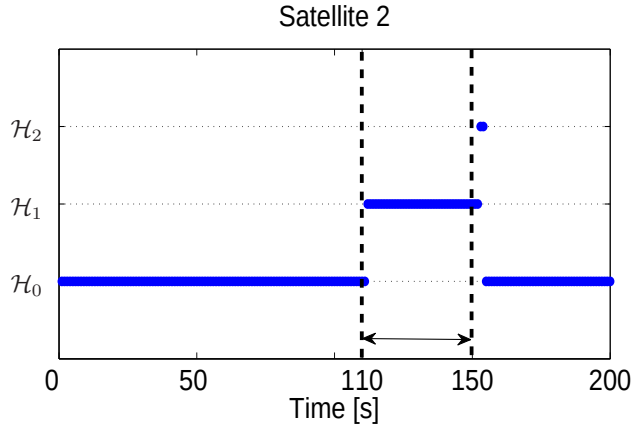

(b)

Fig. 4. Error identification for the two interfered satellites. Dashed lines contain time intervals where errors are present.

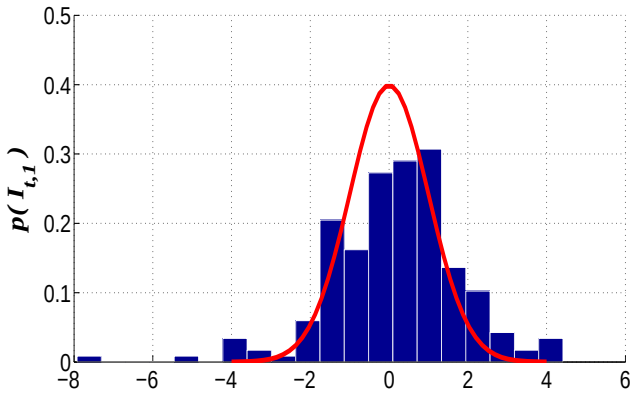

(a) Standard EKF

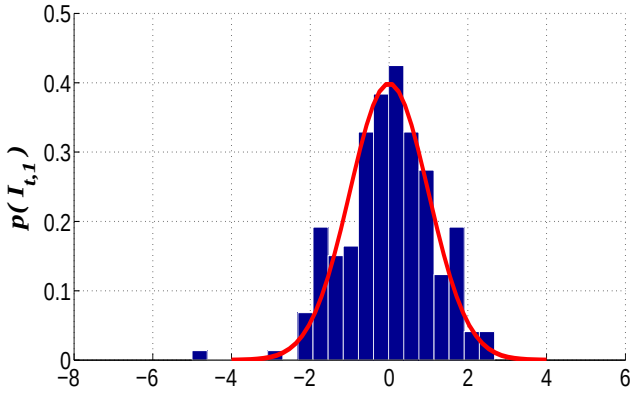

(b) Proposed detection/identification/correction algorithm

Fig. 5. Innovation distributions for satellite 1.

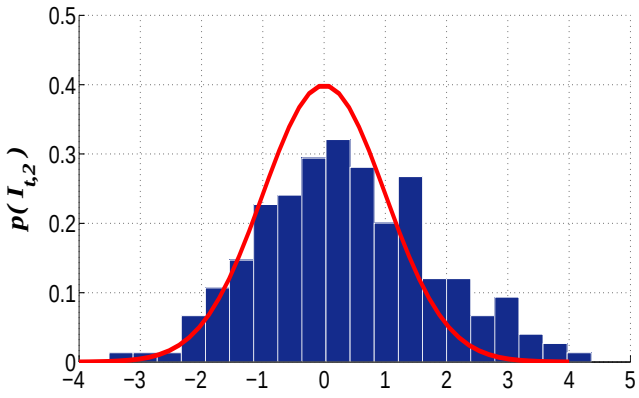

(a) Standard EKF

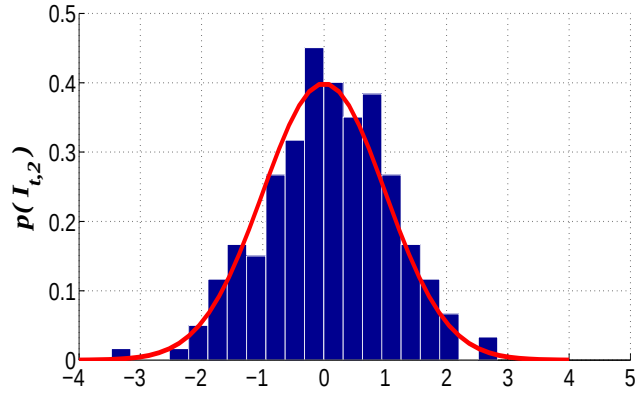

(b) Proposed detection/identification/correction algorithm

Fig. 6. Innovation distributions for satellite 2.

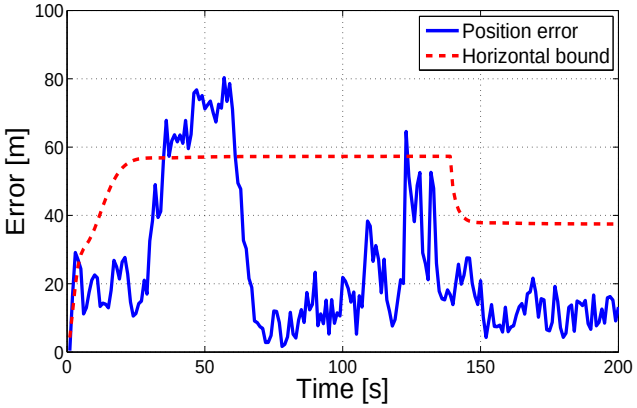

(a) Standard EKF

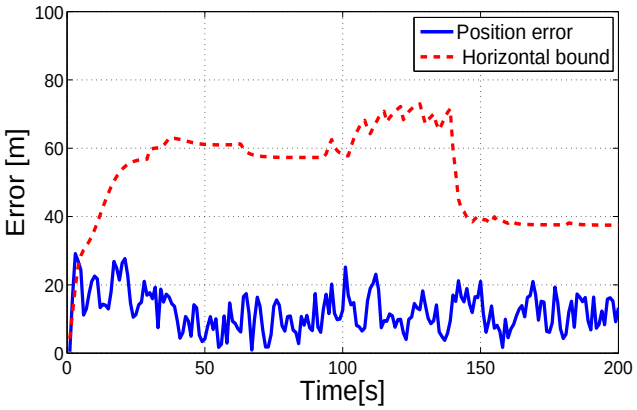

(b) Proposed detection/identification/correction algorithm

Fig. 7. Final position errors (solid line) and horizontal bounds (dashed line).

Fig. 8. Vehicle circuit in Toulouse centre.

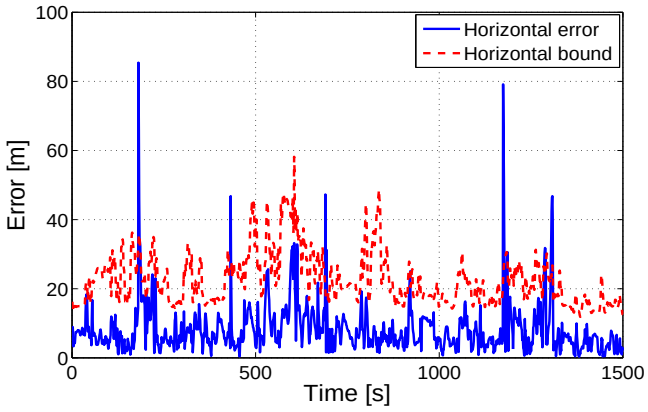

(a) Standard EKF

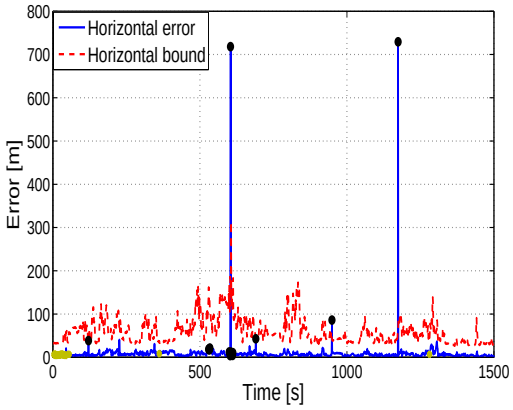

(b) RAIM+FDE strategy

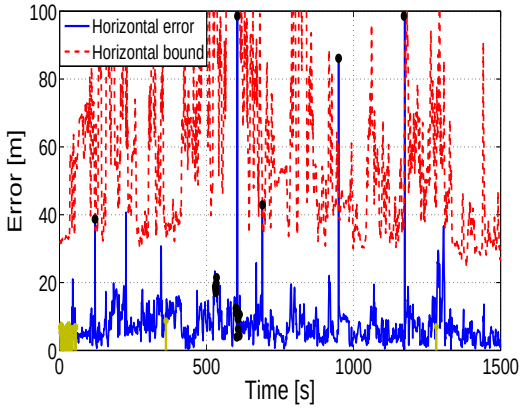

(c) Zoomed RAIM+FDE

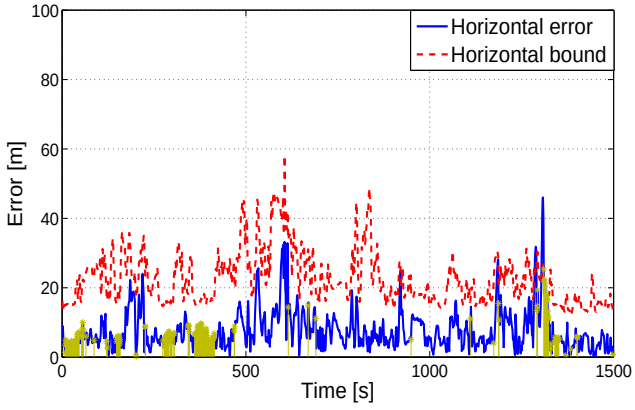

(d) Proposed detection/identification/correction algorithm

Fig. 9. Position errors (solid line) and horizontal bounds (dashed line) with GPS measurements. For the error control strategies (b-c) and (d), the instants where a correction took place are shown as shaded areas under the position error curve.

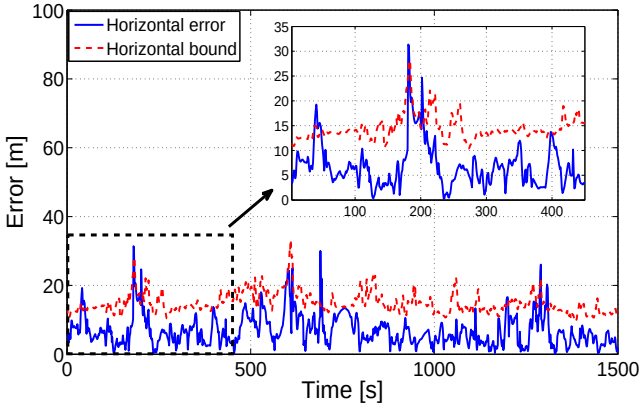

(a) Standard EKF

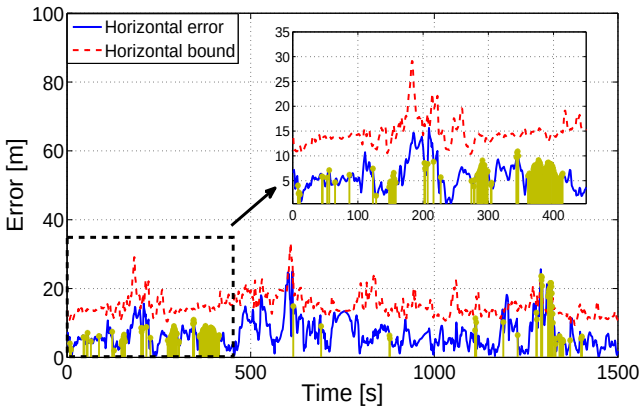

(b) Proposed detection/identification/correction algorithm

Fig. 10. Position errors (solid line) and horizontal bounds (dashed line) with GPS+DR measurements. For the error control strategy (b), the instants where a correction took place are shown as shaded areas under the position error curve.